JACS
JOURNAL OF THE AMERICAN CHEMICAL SOCIETY
Article
pubs.acs.org/JACS

Structural Basis of the Green−Blue Color Switching in Proteorhodopsin as Determined by NMR Spectroscopy

Jiafei Mao,[†] Nhu-Nguyen Do,[†] Frank Scholz,[‡] Lenica Reggie,[†] Michaela Mehler,[†] Andrea Lakatos,[†] Yean-Sin Ong,[†] Sandra J. Ullrich,[†] Lynda J. Brown,[§] Richard C. D. Brown,[§] Johanna Becker-Baldus,[†] Josef Wachtveitl,[‡] and Clemens Glaubitz*,[†]

[†]Institute of Biophysical Chemistry and Centre for Biomolecular Magnetic Resonance, Goethe University Frankfurt, 60438 Frankfurt am Main, Germany

[‡]Institute of Physical and Theoretical Chemistry, Goethe University Frankfurt, 60438 Frankfurt am Main, Germany

[§]Department of Chemistry, University of Southampton, Southampton SO17 1BJ, United Kingdom

Supporting Information

ABSTRACT: Proteorhodopsins (PRs) found in marine microbes are the most abundant retinal-based photoreceptors on this planet. PR variants show high levels of environmental adaptation, as their colors are tuned to the optimal wavelength of available light. The two major green and blue subfamilies can be interconverted through a L/Q point mutation at position 105. Here we reveal the structural basis behind this intriguing color-tuning effect. High-field solid-state NMR spectroscopy was used to visualize structural changes within green PR directly within the lipid bilayer upon introduction of the green−blue L105Q mutation. The observed effects are localized within the binding pocket and close to retinal carbons C14 and C15. Subsequently, magic-angle spinning (MAS) NMR spectroscopy with sensitivity enhancement by dynamic nuclear polarization (DNP) was applied to determine precisely the retinal structure around C14−C15. Upon mutation, a significantly stretched C14−C15 bond, deshielding of C15, and a slight alteration of the retinal chain's out-of-plane twist was observed. The L105Q blue switch therefore acts locally on the retinal itself and induces a conjugation defect between the isomerization region and the imine linkage. Consequently, the S_0−S_1 energy gap increases, resulting in the observed blue shift. The distortion of the chromophore structure also offers an explanation for the elongated primary reaction detected by pump−probe spectroscopy, while chemical shift perturbations within the protein can be linked to the elongation of late-photocycle intermediates studied by flash photolysis. Besides resolving a long-standing problem, this study also demonstrates that the combination of data obtained from high-field and DNP-enhanced MAS NMR spectroscopy together with time-resolved optical spectroscopy enables powerful synergies for in-depth functional studies of membrane proteins.

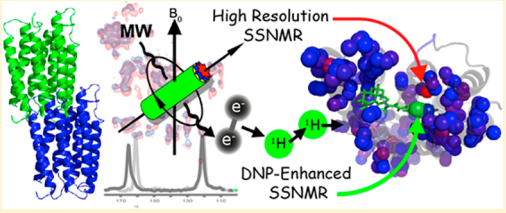

INTRODUCTION

The surprising discovery of proteorhodopsin (PR) represented the first evidence of a bacterial retinal-based photoreceptor.[1] It shows the typical structural scaffold of seven transmembrane helices with the cofactor linked to the protein via a Schiff base and forms large pentameric and hexameric complexes.[2,3] Its identification through metagenomic screens of uncultured sea samples led to the discovery of many hundreds of PR-like sequences distributed in numerous microorganisms from different geographic areas.[4−6] Their prevalent occurrence in microbial communities in the ocean's photic zone and their ability to act as light-driven proton pumps,[7] which create a transmembrane electrochemical gradient, make retinal-based phototrophy a very important bioenergetic factor in marine ecosystems during nutrient-deficient periods.[8,9] PR has been extensively studied through the concerted application of advanced biophysical methods, including, e.g., time-resolved optical spectroscopy,[10] atomic force microscopy,[3] Raman and infrared spectroscopy,[11] liquid-[12] and solid-state NMR spectroscopy,[13,14] dynamic nuclear polarization (DNP) experiments,[15,16] electron paramagnetic resonance spectroscopy,[16] and X-ray crystallography,[17] as recently reviewed by Bamann et al.[18]

One of the most intriguing properties of the proteorhodopsin family is their high level of environmental adaptation with respect to optimized absorption of the available light. Two main PR subfamilies that differ significantly in their light absorption profiles have been discovered in nature. Green-light-absorbing PR (GPR, λ_{max} = 525 nm) is mainly distributed in microbes living at the water surface, whereas blue-light-absorbing PR (BPR, λ_{max} = 490 nm) dominates at greater depths.[19] The high sequence similarity between the differently colored PR variants makes this protein family an excellent case for studying general principles of color tuning, as the number of influencing residues is minimized. Understanding the factors controlling spectral tuning is a long-standing problem that has triggered significant research efforts and has attracted additional

Received: September 23, 2014
Published: November 21, 2014

dx.doi.org/10.1021/ja5097946 | J. Am. Chem. Soc. 2014, 136, 17578−17590

attention with the emergence of optogenetics and the desire to engineer retinal proteins with defined optical properties.[20]

Previous genomic analyses and biochemical studies have demonstrated that a single residue at position 105 serves as a major determinant for wavelength regulation in PRs. This residue is a leucine in GPR and a glutamine in BPR (Figure 1),

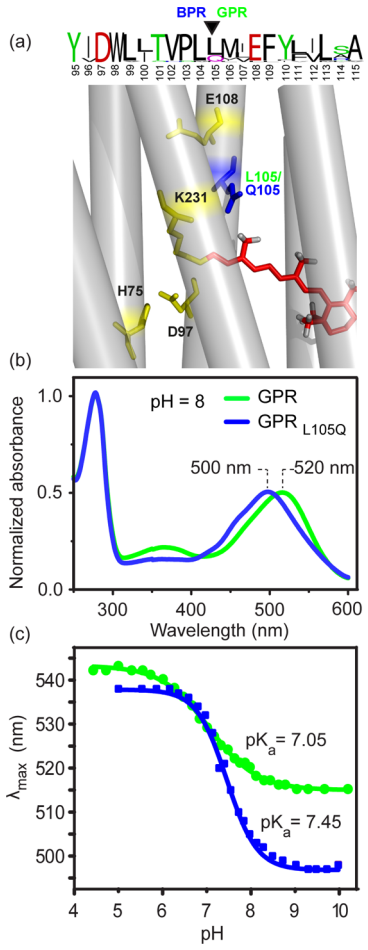

Figure 1. (a) A protein sequence alignment across the PR family shows a leucine for the green variant and a glutamine for the blue variant at position 105 as well as a conserved TxxxL/Q motif at residues 101 through 105. Residue 105 is located in the vicinity of the retinal cofactor.[12,17] Important residues are highlighted in the cartoon (proton donor E108, proton acceptor D97, Schiff base K231, and conserved H75 stabilizing D97). The alignment was generated using WebLOGO. (b) Stationary light absorption spectra of GPR and GPR_{L105Q} at pH 8 reveal a mutation-induced blue shift of 20 nm. (c) A pH titration shows that the observed blue shift is largest above the pK_a of the primary proton acceptor, which is 7.05 and 7.45 for GPR and GPR_{L105Q}, respectively. The pH-dependent color change is more pronounced in GPR_{L105Q}.

and GPR can be switched into BPR with a single L105Q point mutation and vice versa.[19,21] This color switching is also associated with a 10-fold slower photocycle in BPR, which has been suggested to correlate well with the reduced photon flux rate at the depths at which the blue PR gene was found.[22]

A number of attempts were undertaken to explain the mechanism behind this distinct color-tuning effect.[23−28] Solution-state NMR spectroscopy and X-ray crystallography have shown that in both GPR and BPR the side chain of residue 105 is in close proximity to methyl group C20 at the end of the polyene chain.[12,17] The same observation was made for bacteriorhodopsin (BR), in which the corresponding residue L93 shows a similar location and has also been shown to have an effect on the color.[29] Replacing the nonpolar side chain of Leu with the more polar one of Gln increases the polarity within the retinal binding pocket but decreases the side-chain partial molar volume only slightly.[30,31] Interestingly, a recent extensive mutation study demonstrated that λ_{max} shows no correlation with the polarity but is correlated with the side-chain volume of the amino acid at position 105, which does not explain the blue shift induced by L105Q.[28] Therefore, the mechanism behind the naturally occurring green−blue color-switch mutation remains unclear. To resolve this problem, methods have to be applied that allow site-resolved monitoring of mutation effects and enable the detection of very fine structural perturbations within the chromophore−protein complex at sufficient resolution. Such data, which can be provided by solid-state NMR spectroscopy (ssNMR), will also help bridging the gap between quantum-chemical and experimental approaches toward color tuning.

ssNMR offers a versatile approach to analyze structure, dynamics, and functional mechanisms of membrane proteins embedded within lipid bilayers.[32] In particular, the retinal protein field has benefited from cutting-edge ssNMR developments mainly based on magic-angle sample spinning (MAS NMR). It has been shown that the finest perturbation in the sub-Ångstrom range within the retinal cofactor can be determined to high precision, as demonstrated for bovine rhodopsin and BR.[33−36] The availability of high field strengths offers the possibility of extensive resonance assignments on extensively labeled samples needed for further structure and dynamics analysis.[14,37,38] In favorable cases, even a 3D structure determination is possible, as shown for *Anabaena* sensory rhodopsin.[39] The combination of DNP with MAS NMR has brought an essential improvement in sensitivity by orders of magnitude.[40] This approach has proved to be especially useful for hypothesis-driven site-specific problems that require work under cryogenic conditions, as demonstrated for BR and other membrane proteins.[15,41−43] In case of PR, ssNMR has made essential contributions including basic studies on retinal and protonated Schiff base,[44] unveiling the coupling between His75 and the primary proton acceptor Asp97,[13] secondary structure and dynamics analysis,[14,45,46] and resolving interactions between a distant loop mutation at position A178 and the retinal binding pocket.[15] Some of these studies are also powerful examples of the synergistic interplay between ssNMR and optical spectroscopy and the high complementarity with X-ray crystallography.[13−15]

Here we present an extensive ssNMR study on GPR and its blue mutant GPR_{L105Q}, which corresponds to BPR occurring in nature. Multidimensional MAS NMR experiments (proton-driven spin diffusion (PDSD), NCO, NCA, and N(CA)CX) at very high fields applied to uniformly ^{13}C,^{15}N-labeled samples allowed visualization of mutation-induced rearrangements within GPR via determination of chemical shift perturbations. Additional deuteration of GPR enabled the investigation of retinal−protein contacts via dipolar $^{1}H-^{13}C$ heteronuclear correlation (HETCOR) experiments. DNP-enhanced MAS NMR was used to probe the effect of the green−blue switch on the retinal structure itself. The C14−C15 bond length and the HCCH torsion angle at the C14−C15 bond were determined using double-quantum (DQ) spectroscopy. All of our data converge onto a molecular picture in which the interaction

dx.doi.org/10.1021/ja5097946 | J. Am. Chem. Soc. 2014, 136, 17578−17590

between Q105 and the retinal causes a particular distortion of the chromophore's conjugated π system, altering the S_0 and S_1 states and resulting in a blue shift. Our findings will be discussed in the light of additional time-resolved optical data obtained in the time window from femtoseconds to milliseconds that show a slower primary reaction and elongated lifetime of late-photocycle intermediates.

RESULTS

Stationary and Time-Resolved Optical Spectroscopy of GPR and GPR_{L105Q}. A series of pH-dependent absorption spectra of GPR and GPR_{L105Q} solubilized in *n*-dodecyl-β-D-maltoside (DDM) were recorded (Figure 1b,c). At pH 8, a mutation-induced 20 nm blue shift from λ_{max} = 520 to 500 nm is observed. The absorption maximum λ_{max} depends on the protonation state of the primary proton acceptor D97.[47] For GPR, λ_{max} shifts from 515 to 540 nm ($\Delta\lambda$ = 25 nm) as the pH is lowered from 10 to 4. GPR_{L105Q} follows this trend, but λ_{max} changes over a wider range from 537 to 495 nm ($\Delta\lambda$ = 42 nm). The blue shift is especially pronounced at pH values above the pK_a of the primary proton acceptor D97, which can be obtained from the inflection point of the sigmoidal titration curves and was found to be 7.05 for GPR and 7.45 for GPR_{L105Q}.

We probed the dynamics of the primary photoreaction by time-resolved optical pump−probe spectroscopy in the time range from 100 fs to nanoseconds. The photoisomerization around the C13=C14 double bond and the formation of the K intermediate occur on this time scale. For comparison, time traces for three representative wavelengths where the signal is dominated by either excited-state absorption (ESA) (464 nm), generation of the photoproduct (PA) (556 nm), or stimulated emission (SE) (820 nm) are shown for GPR and GPR_{L105} in Figure 2a. Overall, similar behavior is observed for the two samples, but the L105Q mutation slows down the primary reaction in a complex way. The data could be simulated with a sum of four exponential decays (Table 1).

Flash photolysis was then used to analyze mutation-induced alterations in the slower photocycle dynamics on a time scale of 1 μs to 20 s after photoexcitation. The transient absorption changes for GPR and GPR_{L105Q} after photoexcitation are shown in Figure 2b. At 590 nm, a decrease in the positive absorption signal in GPR is observed as a result of the decay of the K intermediate, which is the photoproduct of the primary reaction observed in the pump−probe measurements mentioned above. This decay is accompanied by an increasing absorption monitored at 400 nm caused by the formation of a deprotonated Schiff base species (the M intermediate). The subsequent formation of the late intermediates N and O is indicated by an absorption increase at 590 nm. These species decay simultaneously while the signal at 510 nm grows, which indicates the repopulation of the initial state. In contrast, the photodynamics of GPR_{L105Q} is strongly altered. The amplitude at 560 nm is almost constant up to 100 μs, which means that the K state has already decayed and is not detected within the time window accessible by flash photolysis. Interestingly, the M state observed through absorbance changes at 370 nm is not populated earlier, but its lifetime is significantly reduced. The subsequent formation of the late intermediates N and O at 560 nm is also strongly affected, showing a complex behavior with an extended lifetime. This is further confirmed by the dramatically delayed repopulation of the initial ground state monitored at 480 nm. A global fit analysis revealed that the data could be described by five exponential functions. A comparison with GPR is given in Table 1.

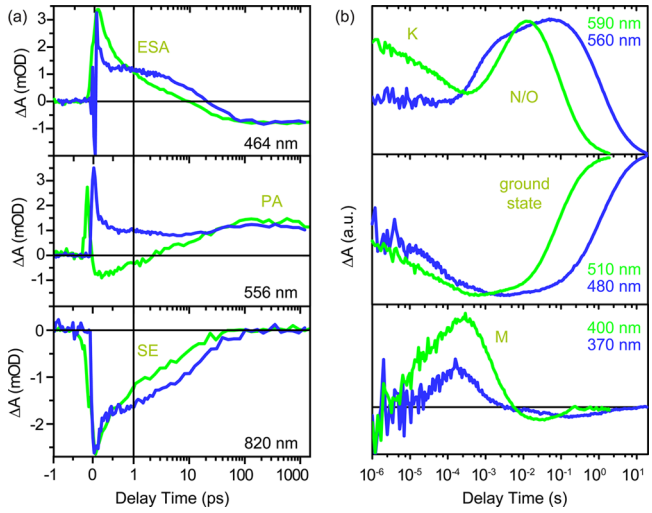

Figure 2. (a) Time traces of the primary photoreaction for GPR and GPR_{L105Q} at pH 9. The absorption changes at 464, 556, and 820 nm are dominated by excited-state absorption (ESA), photoproduct formation (PA), and stimulated emission (SE), respectively. Lifetimes were extracted from these curves by fitting four exponential decays (Table 1). (b) Laser-flash-induced transient absorption changes at pH 9 for GPR and GPR_{L105Q} on a time scale of 1 μs to 20 s. The transients are representative of (middle) the dynamics of the ground-state population (510 nm/480 nm), (top) the decay of the K intermediate at early delay times and the formation and decay of the N and O intermediates at late delay times (590 nm/560 nm), and (bottom) the formation and decay of the M intermediate (400 nm/370 nm).

Mutation-Induced Chemical Shift Changes in GPR Determined by $^{13}C-^{13}C$ and $^{13}C-^{15}N$ MAS NMR. In order to identify structural changes induced by the green−blue L105Q mutation, we characterized GPR and GPR_{L105Q} embedded in lipid bilayers by MAS NMR at high field (ν_0^{1H} = 850 MHz). For chemical shift assignment, several dipolar-based $^{13}C-^{13}C$ and $^{15}N-^{13}C$ spectra on uniformly ^{13}C,^{15}N-labeled samples were acquired. The aromatic residues are abundant in integral membrane proteins and often show highly overlapping side-chain signals. Therefore, in order to simplify the spectral analysis, signals from Phe, Tyr, and Trp as well as those from two other abundant and hydrophobic residues (Leu and Val) were suppressed by reverse labeling. As shown in Figure S1 in the Supporting Information, the majority of the peaks in $^{13}C-^{13}C$ PDSD and NCA spectra of GPR and GPR_{L105Q} are superimposable. This indicates that these two proteins have highly similar secondary structures.

From the known chemical shift assignments of GPR[45] as a starting point, a number of residues of GPR_{L105Q} in the $^{13}C-^{13}C$ PDSD, NCA, and N(CA)CX spectra were unambiguously identified, which enabled the analysis of mutation-induced chemical shift differences (Table S1 in the Supporting Information). Most of the observed changes were smaller than 0.2 ppm, which means that no major mutation-induced alterations in secondary structure or side-chain conformations occurred. However, a small set of 10 residues (T69, E85, T101, I112, A115, A116, I145, A185, T188, and I194) was found to show unambiguous ^{13}C chemical shift changes on the side chain and/or backbone that were larger than the average chemical shift difference of 0.4 ppm. Available structural data

dx.doi.org/10.1021/ja5097946 | J. Am. Chem. Soc. 2014, 136, 17578−17590

Table 1. Optical Properties of GPR and GPR_{L105Q} in DDM Micelles

				primary reaction (ps)[c]				photocycle (ms)[d]				
	λ_{max} (nm)[a]	$\Delta\lambda$ (nm)[b]	pK_a	τ_1	τ_2	τ_3	τ_4	t_1 (K → M)	t_2 (M → N)	t_3 (N → O)	t_4 (O → PR)	t_5 (O → PR)
GPR[e]	520	25	7.05	0.15	0.28	9.5	>1000	0.07	1	5.2	44	210
GPR_{L105Q}	500	42	7.45	0.13	2.3	24	>1000	0.06[f]	0.7	23	83	3800

[a]pH 8. [b]pH 4 to pH 10. [c]Time constants for the primary reaction at pH 9 obtained from global fit analyses of the data shown in Figure 2a using a sum of four exponentials for all wavelengths with different amplitudes. [d]Time constants for slower steps of the photocycle at pH 9 as determined by global fit analyses of the flash photolysis data in Figure 2b using a sum of five exponential functions. [e]Data from Hempelmann et al.[13] [f]The time constant does not show a significant amplitude in the spectral range of the K state (Figure 2b, top), indicating decay of this photointermediate on a shorter time scale.

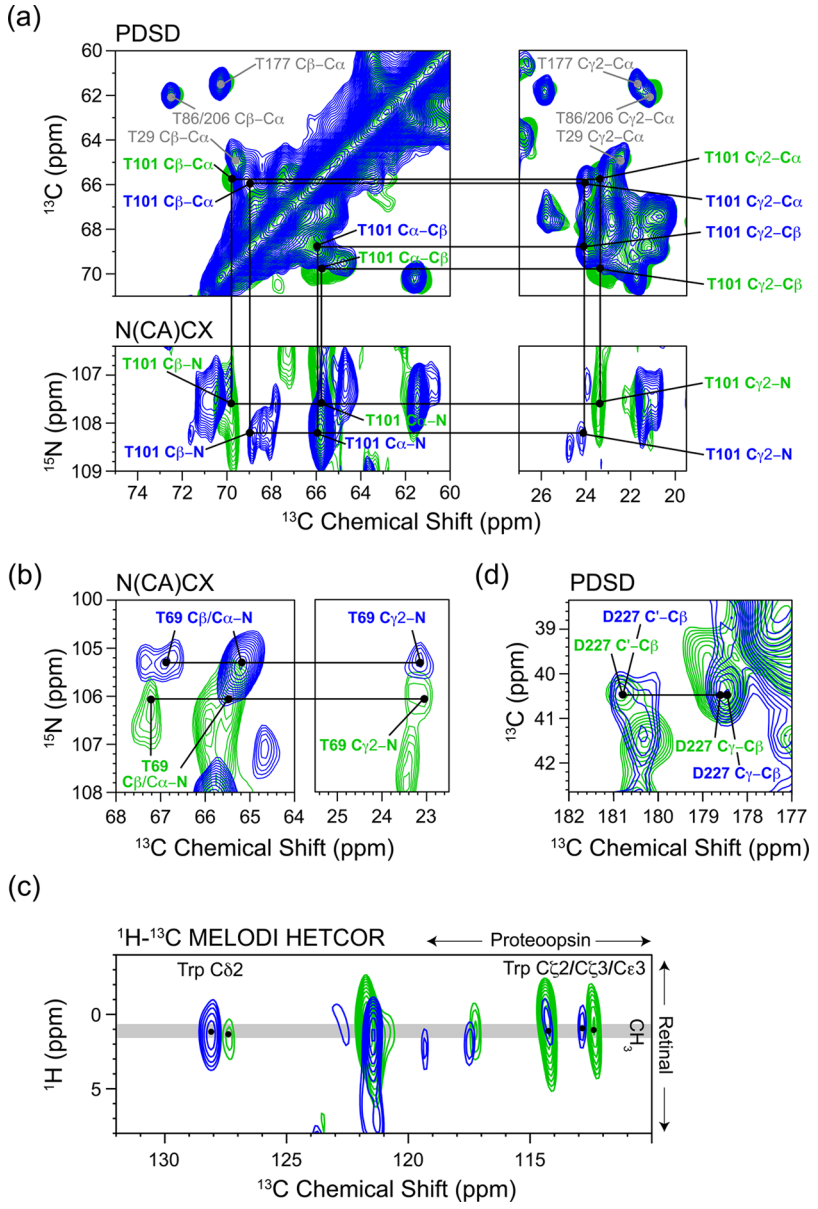

Figure 3. Chemical shifts of residues close to site 105 and/or in the retinal binding pocket are significantly perturbed by the L105Q mutation. (a) The largest effect is observed for T101, as identified in the ^{13}C–^{13}C PDSD (20 ms mixing time) and ^{15}N–^{13}C N(CA)CX MAS NMR spectra, while other Thr residues shown in the same spectral region are not affected. (b, c) Further effects are observed, for example, for (b) T69 in a N(CA)CX spectrum and (c) W197 in a ^{1}H–^{13}C HETCOR spectrum. (d) In contrast, D227 and D97, which are part of the counterion complex to the protonated Schiff base, are not influenced (PDSD of 20 ms mixing time). Spectra are color-coded (green = GPR, blue = GPR_{L105Q}). See the text for further experimental details and labeling schemes used.

for different PR variants based on X-ray crystallography or liquid-state NMR reveal that residues T69, T101, and I194 are located within or close to the retinal binding site.[12,17] Example spectra showing significant chemical shift changes for T101 and T69 are presented in Figure 3a,b. The largest chemical shift change (0.8 ppm) was observed for Cβ of the T101 side chain,

dx.doi.org/10.1021/ja5097946 | J. Am. Chem. Soc. 2014, 136, 17578–17590

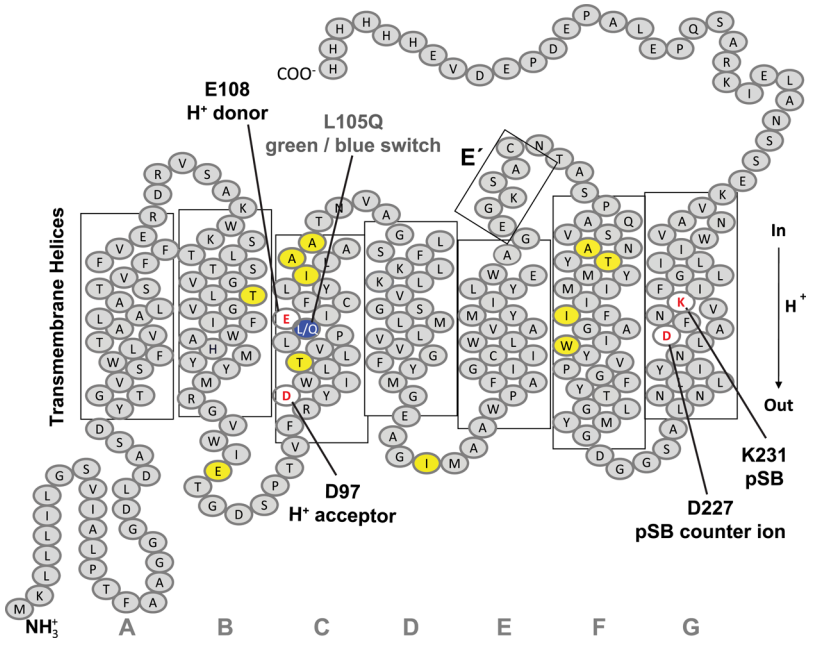

Figure 4. Topology plot with a summary of all observed chemical shift perturbations in GPR upon L105Q mutation. The mutation site is colored in blue, and residues showing significant ^{13}C chemical shift changes (>0.4 ppm) including T69, E85, T101, I112, A115, A116, I145, A185, T188, I194 and W197, are highlighted in yellow. Some functionally relevant residues (proton acceptor D97, D227, proton donor E108, pSB residue K231) are colored in white.

which comes close to the retinal. In contrast, only small chemical shift changes were found for the side chains of D97 and D227, which serve as the primary proton acceptor and counterions to the protonated Schiff base (pSB) (Figure 3d). The ^{15}N chemical shift of the pSB at pH 9 (181 ppm) is also not affected by the L105Q mutation (Figure 5a), and a comparison with the corresponding values from Schiff base–counterion model complexes and their correlation with λ_{max} shows that GPR deviates from the free retinal systems more than GPR_{L105Q} (Figure 5b). Furthermore, the ^{15}N chemical shift of Nε2 of His75, which forms a unique cluster with D97,[13] remains unchanged (162 ppm; Figure 5a). These data show that the L105Q mutation mainly influences residues in close proximity to the retinylidene chromophore. The locations of all residues for which a significant mutation-induced chemical shift change was observed are highlighted in the GPR topology plot shown in Figure 4.

Mutation-Induced Alterations of Chromophore–Protein Contacts in GPR Detected by $^{1}H-^{13}C$ MAS NMR. The mapping of mutation-induced chemical shift changes described above excludes aromatic residues, which are, however, found in the retinal binding pocket of PR. In order to detect these residues as well as to probe protein–retinal contacts, we used a method based on the concept of selective interface detection (SIDY) originally designed to observe protein–ligand contacts by ssNMR.[48] Instead of combining a ^{13}C-labeled ligand and unlabeled protein as used in the original version of SIDY, we adopted an alternative labeling scheme in which unlabeled retinal was bound to uniformly $^{13}C,^{2}H$-labeled proteoopsin. Performing a dipolar $^{1}H-^{13}C$ HETCOR experiment on such a sample would in principle return a number of $^{1}H-^{13}C$ cross-peaks as evidence for retinal–protein contacts. This approach is straightforward, as it does not require isotope labeling of the ligand by chemical synthesis. The $^{13}C,^{2}H$-labeled samples were reconstituted into highly deuterated lipids and kept in deuterated buffer in order to minimize the proton background. A long contact time (10 ms) in $^{1}H-^{13}C$ cross-polarization (CP) was used to select long-distance contacts, including those crossing the protein–ligand interface (Figure S2a in the Supporting Information). Small contributions from remaining protons resulting in residual short-distance $^{1}H-^{13}C$ contacts within proteoopsin were eliminated using the MELODI scheme (Figure S2b).[49] The resulting $^{1}H-^{13}C$ MELODI-HETCOR spectrum is shown in Figure 3c. The ^{13}C dimension arises from proteoopsin and the ^{1}H dimension from the bound retinal chromophore. The observed cross-peaks in the ^{1}H-methyl–^{13}C-aromatic region therefore represent long-range through-space contacts between the protein and the cofactor. The ^{13}C chemical shifts at 112.4 and 114.3 ppm are characteristic of indole carbons of tryptophan. On the basis of the X-ray crystallographic structures of PR (Protein Data Bank (PDB) entry 4JQ6) and BR (PDB entry 1C3W), we assign these peaks to the conserved contacts between carbons Cζ2, Cζ3, and Cε3 of Trp197 and the protons of the C19 and C20 methyl groups of retinal (Figure S2c). These two peaks become significantly weaker in the spectrum of GPR_{L105Q}, whereas an intense peak at a ^{13}C chemical shift of 127.9 ppm appears, which could be tentatively assigned to Cδ2 of a Trp ring. These observations indicate a slight rearrangement of the Trp ring position relative to the methyl groups on the polyene chain.

Mutation-Induced Structural Changes within the Chromophore Detected by DNP-Enhanced MAS NMR. Our data show that the green–blue L105Q mutation causes very specific effects within the retinal binding pocket close to retinal carbons C14 and C15. Therefore, two samples of U-^{15}N GPR and GPR_{L105Q} in which the retinal cofactor was doubly ^{13}C-labeled at these positions were prepared. Because of the low sample amount restricted by the availability of synthetically labeled retinal, signal enhancement is required in order to obtain an acceptable signal-to-noise-ratio. Furthermore, NMR under cryogenic conditions is needed for the precise

dx.doi.org/10.1021/ja5097946 | J. Am. Chem. Soc. 2014, 136, 17578–17590

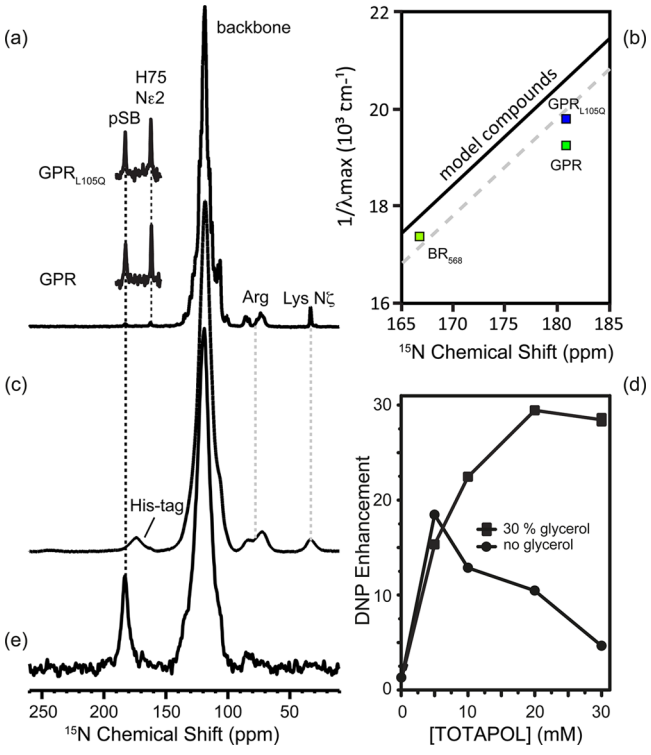

Figure 5. (a) ^{15}N-CP MAS NMR spectrum of U-^{15}N GPR recorded at 280 K. The characteristic ^{15}N signals of the pSB (181 ppm) and Nε2 of His75 (162 ppm) are not affected upon L105Q mutation. (b) Correlation between λ_{max} and pSB ^{15}N chemical shifts obtained from retinal derivatives with all-trans polyene chains with different halide counterions[81] in comparison with BR, GPR, and GPR$_{L105Q}$. (c) ^{15}N CP MAS NMR spectrum of U-^{15}N GPR recorded under DNP conditions at 100 K with e^- and ^{1}H Larmor frequencies of 258 GHz and 393 MHz, respectively. (d) Screening of different sample conditions showed that a maximum of 30-fold signal enhancement could be obtained using 20 mM TOTAPOL in a 30:60:10 glycerol-d_8/D_2O/H_2O mixture. The DNP enhancement was determined from the ^{15}N backbone resonance and calculated according to $I_{mw\ on}/I_{mw\ off}$. (e) DNP-enhanced ^{13}C−^{15}N double CP experiment on [14,15-^{13}C-all-*trans*-retinal,U-^{15}N] GPR. In this experiment, magnetization is transferred from protons to ^{13}C-labeled retinal carbons C14 and C15 and further from C15 to the ^{15}N-labeled nitrogen of the pSB. Its resonance under DNP conditions is slightly broadened but occurs at the same chemical shift compared with the signal recorded at 280 K. It cannot be detected in a conventional DNP-enhanced ^{1}H−^{15}N CP spectrum (c) because the broad peak of the frozen His tag at 170 ppm covers both the pSB and His75 Nε2 signals.

determination of dipole couplings. We therefore used DNP in combination with MAS NMR.

DNP requires sample doping with suitable polarizing agents and their dispersal in a glycerol−water matrix, which forms a glass phase under cryogenic conditions (100 K). The optimal conditions for achieving the best possible enhancement are sample-dependent and require careful adjustment according to the nature of the samples. Here the biradical TOTAPOL[50] was used, and the DNP enhancement was monitored via ^{1}H−^{15}N cross-polarization. In an initial approach, TOTAPOL was directly added into the protein/detergent/lipid reconstitution mixture, attempting to maintain an equal radical concentrations inside and outside of proteoliposomes. This strategy was not successful since TOTAPOL was absorbed by the biobeads used for detergent removal. We therefore soaked the proteoliposome pellet directly in the appropriate radical solution. Samples were incubated for some hours before they were transferred into a MAS rotor. Without glycerol, the best enhancement (18×) was achieved at 5 mM TOTAPOL, while in the presence of 30% glycerol (30:60:10 glycerol-d_8/D_2O/H_2O) an up to 30-fold enhancement at 20 mM TOTAPOL was detected (Figure 5c,d). Further increasing the glycerol concentration did not provide any improved enhancement and was therefore avoided. Figure 5a,c compares a conventional ^{15}N CP MAS NMR spectrum of U-^{15}N GPR with a DNP-enhanced spectrum. As described above, a significant signal enhancement was achieved, but some line broadening due to the low operation temperature needed for DNP (100 K) was observed as well. The ^{15}N signals of pSB and H75 are covered by a broad signal centered on 170 ppm that probably arises from the His tag. The His tag is usually not observed in nonfrozen GPR samples above pH 7.5 but cross-polarizes under cryogenic conditions. Since the sample carries 14,15-^{13}C-all-*trans*-retinal, the pSB signal can be cleanly filtered out by two cross-polarization steps in which ^{1}H magnetization is transferred first to C14 and C15 and from there to the directly bonded ^{15}N of the pSB (Figure 5e). The remaining backbone signal arises from HCN double-CP transfers between ^{15}N and natural-abundance ^{13}C within PR. As shown in Figure 5e, the chemical shift of the pSB ^{15}Nε in GPR is observed at 181 ppm, which is identical to room-temperature measurements (Figure 5a). This signal is broadened, but the identical chemical shift indicates an intact and functional state, in line with earlier cryo-FTIR studies.[51]

DNP-enhanced ^{1}H−^{13}C CP MAS NMR spectra of 14,15-^{13}C-retinal bound to U-^{15}N PR are shown in Figure 6. A 27-fold enhancement using the conditions described above was achieved, allowing detection of the C14 and C15 signals even when using as little as 1 mg of protein sample and with a much reduced experimental time. All of the natural-abundance signals were removed upon application of a dipolar double-quantum filter (DQF). The two remaining resonances are assigned to C14 and C15 of the retinal cofactor. For GPR, the resonances of C14 and C15 are observed at 120 and 161 ppm, respectively. The line widths of these two peaks are 184 and 159 Hz, respectively, which are both larger than the upper limit of the homogeneous line width converted from refocused single-quantum coherence lifetimes (Figure S3 in the Supporting Information). Chemical shift changes are observed in the L105Q mutant, as C14 shifts to 121.3 ppm and C15 to 165.4 ppm (Figure 6b). In both constructs, the chemical shifts of these two sites (Table 2) clearly point to a single all-trans conformation of retinal in the ground state.

We further analyzed DQ buildup curves to determine the exact bond length between C14 and C15 (Figure 7a−c). We adapted a standard POST-C7-based DQ scheme and monitored the signal intensity while varying the DQ excitation and reconversion steps simultaneously.[33] It has been shown that this method is able to precisely determine internuclear distances and is rather sensitive to small bond-length alterations. For GPR, a dipole coupling of 2665 Hz was found, corresponding to a bond length of 142 pm, which is significantly shorter than the 146 pm expected for an ideal single-bond length in linear polyene systems, as found in crystalline all-*trans*-retinal.[52] In contrast, a dipolar coupling of 2450 Hz, resulting in a bond length of 146 pm, was determined for GPR$_{L105Q}$.

In addition to the C−C bond length, we also determined the planarity around the C14−C15 bond by measuring the H−C14−C15−H dihedral angle. This was achieved by hetero-

dx.doi.org/10.1021/ja5097946 | J. Am. Chem. Soc. 2014, 136, 17578−17590

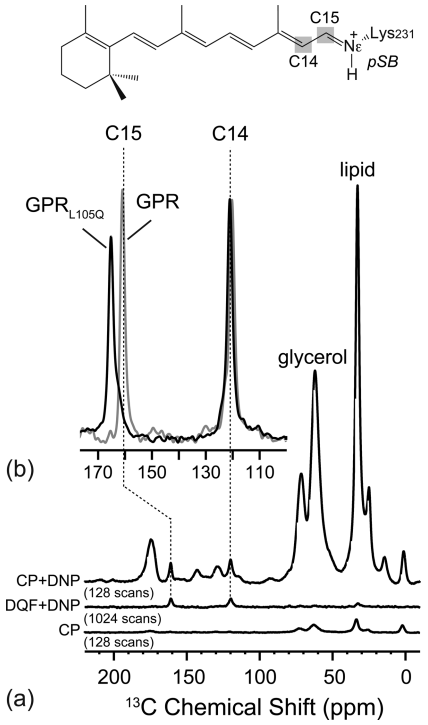

Figure 6. (a) DNP-enhanced ^{13}C CP MAS NMR spectrum of 14,15-^{13}C-all-*trans*-retinal bound to GPR. A 27-fold signal enhancement was achieved, as shown by the spectra recorded with and without DNP. The ^{13}C natural-abundance background from protein, lipids, and glycerol were efficiently suppressed by a double-quantum filter (DQF). (b) Comparison of DNP-enhanced DQF ^{13}C NMR spectra of 14,15-^{13}C-all-*trans*-retinal in GPR and GPR$_{L105Q}$. Upon L105Q mutation, the C14 chemical shift changes slightly from 120.2 to 121.3 ppm and the C15 signal shifts significantly from 161.1 to 165.4 ppm.

nuclear local field (HLF) experiments, which spectroscopically "isolate" this fragment from the environment and have been successfully applied on biological solids.[53,54] Here we chose a recently released version of HLF-HCCH experiments that uses twice the dipolar phase accumulation time of the original version.[53] This method reduces the systematic error by improving the angular resolution of the measurements and also raising the number of acquirable data points and is therefore better suited for determining the fine structural details required here. Experimental and simulated dephasing curves are shown in Figure 7d,e. For GPR, a best fit was obtained for 161°, which changes to 164° in GPR$_{L105Q}$. Therefore, this moiety adopts a translike conformation in both proteins. However, the measured values still differ significantly from an ideal trans conformation by 16−19°. This deviation, which does not exist in all-*trans*-retinal in solution, may be due to steric effects from the protein environment, as also found in BR.[54]

DISCUSSION

Optical spectroscopy shows that the L105Q mutation in green proteorhodopsin causes a significant blue shift of 20 nm at pH 8 (Figure 1b), as observed for native blue proteorhodopsin.[19,21] This color tuning is accompanied by a slower primary reaction and extended lifetimes of late-photocycle intermediates (Figure 2a,b). The approximately 10-fold slower photocycle of GPR$_{L105Q}$ resembles the characteristics of naturally occurring BPR.[19,21,22] GPR therefore offers an excellent platform for understanding the molecular basis of this mutation-induced color tuning. Detergent/lipid effects or an altered oligomeric state of GPR$_{L105Q}$ compared with GPR can be excluded as the source of the color shift, as the two samples were prepared and studied under identical conditions and both form oligomeric complexes of the same size (Figure S4 in the Supporting Information). Despite the known location of the mutation site in close proximity to methyl group C20 at the end of the polyene chain[12,17] and numerous spectroscopic and biochemical studies,[23−28] the underlying mechanism of the observed color shift remained unclear, which emphasizes the need to use high-resolution and high-precision methods such as ssNMR to answer this key question.

Mutation-Induced Chemical Shift Perturbations Visualize Highly Localized Structural Effects on GPR. We have identified unambiguous mutation-induced chemical shift changes in a small number of residues. Their locations within the topology plot are shown in Figure 4. Most of them are found close to the mutation site in helices C and F. The small number of affected sites indicates a highly location-specific effect. This is in contrast to another color-tuning mutation, A178R within the EF loop, which causes a large number of chemical shift perturbations starting from the EF loop and spreading throughout the whole protein.[15] The most pronounced chemical shift change is observed in the side chain of residue T101 close to the end of the retinal polyene chain (Figure 8a). This residue is located just beneath L105 on the same side of helix C pointing toward the retinal chromophore (Figure 8b). This observation reveals a significant coupling between the two sites. Interestingly, this TxxxL motif (Figure 1a) seems to be conserved, as it is found not only in PR but also in BR and xanthorhodopsin.[55] The chemical shift perturbations do not propagate further along helix C. The primary proton acceptor D97 located below T101 and the primary proton donor E108 above L105 are not affected by the L105Q mutation. It appears that the structural changes triggered by this mutation do not extend more than two turns toward the extracellular direction. Similarly, no significant perturbations are observed for the pSB K231 or for D227 (Figure 8b). The occurrence of primarily short-range interactions is also seen for chemical shift changes of W197 close the L105Q site, which do not extend to M134 on the retinal-facing side of helix D (Figure 8b). Interestingly, Q105 and W197 were shown to interact via hydrogen-bonded water

Table 2. NMR Parameters for the Chromophores in GPR and GPR$_{L105Q}$

	pSB ^{15}N chemical shift (ppm)	^{13}C chemical shifts (ppm)		C14−C15 dipolar coupling constant (Hz)	C14−C15 bond length (pm)	H−C14−C15−H dihedral angle (deg)
		C14	C15			
GPR	181	120.2	161.1	2665 ± 40	142 ± 1	161 ± 3
GPR$_{L105Q}$	181	121.3	165.4	2450 ± 45	146 ± 1	164 ± 2

dx.doi.org/10.1021/ja5097946 | J. Am. Chem. Soc. 2014, 136, 17578−17590

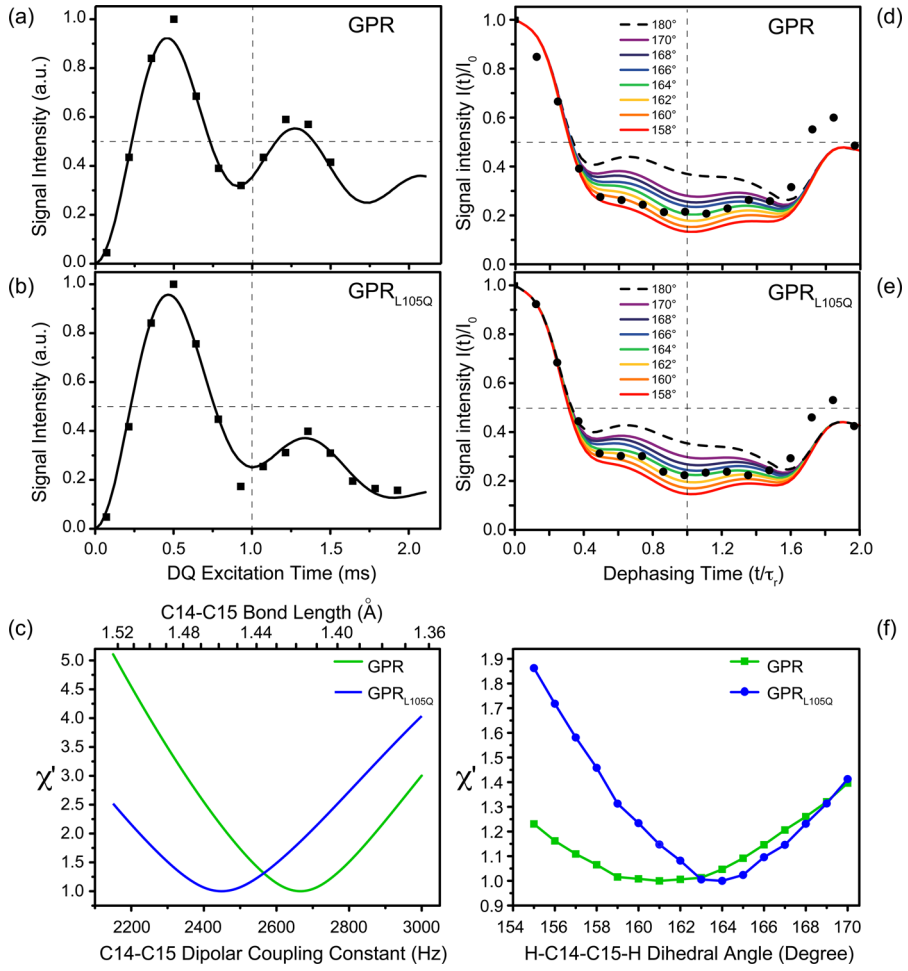

Figure 7. Determination of the retinal conformation at the C14−C15 position by double-quantum spectroscopy under DNP-enhanced MAS NMR conditions. (a, b) Double-quantum coherence buildup curves for 14,15-^{13}C-all-*trans*-retinal in (a) GPR and (b) GPR$_{L105Q}$ were obtained using POST-C7. (c) The data are well-described by ^{13}C−^{13}C dipolar couplings of 2665 ± 40 Hz (142 ± 1 pm) and 2450 ± 45 Hz (146 ± 1 pm) for GPR and GRP$_{L105Q}$, respectively. (d, e) HLF-HCCH dephasing curves for the C14−C15 spin systems in (d) GPR and (e) GPR$_{L105Q}$ reporting on the HCCH torsion angle. (f) Subtle differences are observed, with the angle changing from 161 ± 3° in GPR to 164 ± 2° in GPR$_{L105Q}$. All of the spin dynamics simulations were performed using SIMPSON. The experimentally observed transverse relaxation was taken into account by including a monoexponentially decaying function in the simulations. See Materials and Methods for further details.

molecules in some of the protomers of the BPR X-ray structure.[17]

Structural Basis of the Green−Blue Switch in Proteorhodopsin. In general, color tuning (i.e., the opsin shift) depends on a number of mechanisms that affect the delocalization of the positive charge at the protonated Schiff base along the polyene chain and the S_0-S_1 gap.[56−58] Contributing factors include (i) the orientation of the cyclohexene ring, (ii) an altered counterion−Schiff base distance, and (iii) structural and electronic distortions of the retinal polyene chain itself caused by local steric or electrostatic effects.

(i) Alterations in the cyclohexene ring/polyene chain coplanarity can contribute up to 20% of the opsin shift[59] and are mainly determined by altered protein−ring contacts. Such an effect does not seem likely in our case, since no chemical shift changes in residues surrounding the cyclohexane ring were observed, which would be indicative of structural rearrangements. This is in contrast to the red-shifting A178R mutation, which triggers chemical shift changes within residues surrounding the ring, showing that the binding pocket is allosterically regulated by the distal EF loop.[15]

(ii) The electrostatic effect caused by an altered distance between the protonated Schiff base and the counterion is a major color-determining factor. The ^{15}N chemical shift of the pSB nitrogen is highly sensitive to the formation of hydrogen bonds, the dielectric properties of its surrounding vicinity, and the counterion distance. It can be directly linked to λ_{max} of the retinal pigment[60,61] (Figure 5b). However, the L105Q mutation affects neither the chemical shift of the pSB nitrogen nor its interacting residues D97 and D227, which are part of the counterion complex. Moreover, H75, a residue involved in hydrogen bonding with D97,[13] remains unaffected, and the pK_a of D97 increases only slightly. Previous studies hypothesized that the green−blue switching in GPR is based on an altered pSB environment.[19,26,28] Our data show that the net effect of the protein environment on the pSB nitrogen seems rather similar in GPR compared to its blue version. Therefore, altered counterion effects are probably not a major determinant of the L105Q-mutation-induced blue shift.

(iii) The mutation-induced chemical shift perturbations point toward a protein-induced structural rearrangement within the retinal close to the end of its polyene chain (Figure 8a). To gain deeper insight into alterations within this part of the

dx.doi.org/10.1021/ja5097946 | J. Am. Chem. Soc. 2014, 136, 17578−17590

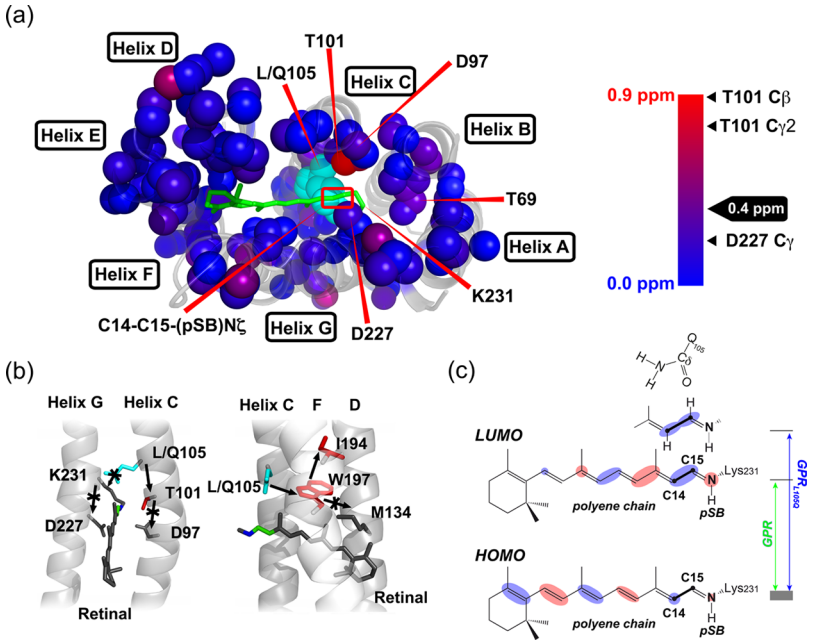

Figure 8. Illustration of the molecular consequences of the L105Q mutation leading to the observed blue shift in GPR. (a) Only subtle structural changes occur, as identified by ^{13}C chemical shift perturbations. Their 3D localization is visualized here by different colors using the BPR X-ray structure (PBD entry 4JQ6), which is shown from the extracellular side.[17] Some loops have been omitted. The average chemical shift change is about 0.4 ppm. The most pronounced effect in the retinal binding pocket is observed for the ^{13}C resonances of the T101 side chain, which is in close proximity to L105/Q105 and close to retinal carbons C14 and C15. (b) These local, mutation-induced changes propagate along helix C and into helices D, F, and G and affect, e.g., T101, W197, and I194 (see Table S1 in the Supporting Information). No effects were observed for the functionally important residues D97, D227, and K231. (c) The carbonyl group of Q105 points toward C15 and the imine linkage. As a consequence of the mutation, the C14−C15 bond is stretched. QM/MM simulations on retinal show a reconfiguration of the conjugated π system between the highest occupied molecular orbital (HOMO) and the lowest unoccupied molecular orbital (LUMO) and a shift toward the pSB, which includes an increase in the π-orbital character of the C14−C15 bond.[66−68] The mutation-induced C14−C15 bond stretching does not alter the bond character in the HOMO but causes an energy increase in the LUMO as the single-bond character increases, which results in a shortened conjugated π system, a larger HOMO−LUMO gap, and therefore a blue shift. Additional factors include the expected extension of the conjugation effect toward the isomerization region as well as electrostatic effects due to the orientation of the polar side chain. The HOMO and LUMO of pSB retinal are represented as simplified cartoons as projected from one side of the molecular plane.[67] Opposite signs of the π-orbital wave functions are colored in blue and red.

chromophore, ^{13}C labels were introduced at positions C14 and C15, and the samples were analyzed using DNP-enhanced MAS NMR to ensure the highest sensitivity, precision, and localization. Upon mutation, deshielding of C15 (Figure 6b) and stretching of the C14−C15 bond by 4 pm (Figure 7c) were observed. Furthermore, we found a significant out-of-plane twist of the H−C14−C15−H torsion angle in both green and blue PR constructs (Figure 7f). Previously, the localization of such a conjugation defect and its relation to the chemical shifts of the odd-numbered carbons have been extensively studied and described for rhodopsin.[62,63] In our case, the observed C14−C15 bond stretching together with the deshielding of C15 show that the conjugation defect induced by the protonated Schiff base covers the end of the polyene chain. This defect could propagate further to the isomerization region, as indeed indicated by the strongly altered isomerization kinetics upon mutation (Figure 2a and Table 1). It is worth noting that previous studies in rhodopsin also support our finding that the conjugation defect could be solely regulated by the polyene chain rather than the ionone ring and Schiff base.[64]

The question is the extent to which this defect is caused by steric or electrostatic interactions and how this would explain the observed blue shift of 0.1 eV. A glutamine at position 105 increases the polarity and hydrogen-bonding options and reduces the side-chain volume slightly. A previous theoretical study based on homology modeling and molecular orbital calculations suggested that Q105 could cause a blue shift by stabilizing the S_0 and S_1 states differently if the side-chain dipole moment points with the carbonyl oxygen toward the imine linkage.[24] The authors also proposed that this orientation would be ensured by a hydrogen bond formed between the Q105 carbonyl group and the proton at the retinal carbon C15. Indeed, the deshielding of C15 observed here would be compatible with the formation of a hydrogen bond, and the X-ray structure of BPR also indicates the correct orientation of the Q105 side chain.[17] The importance of the orientation of a polar side chain in the retinal binding pocket is illustrated by the fact that other computational studies have reported red shifts when a glutamine is placed close to the retinal.[65]

The resulting bond stretching and its consequences can also be considered from the perspective of altered electronic configurations in the retinal pigment upon photoexcitation (Figure 8c).[66−68] The HOMO features a characteristic conjugated π-orbital pattern extending along the polyene chain with its maximum at the cyclohexene ring. This conjugated π system shifts toward the pSB in the LUMO. The energy gap between these two states defines the absorption wavelength. C14−C15 bears single-bond character in the HOMO but tends toward double-bond character in the LUMO. The observed elongation of the C14−C15 bond in GPR_{L105Q} disrupts the delocalization of π electrons at this position in the LUMO and could therefore destabilize this

dx.doi.org/10.1021/ja5097946 | J. Am. Chem. Soc. 2014, 136, 17578−17590

state. In contrast, stretching of the C14−C15 bond does not strongly affect the HOMO (Figure 8c). A conjugation defect also hinders the dislocation of the positive charge, causing an accumulation at the end of the chain, which is in line with the observed deshielding of C15. In the LUMO, the conjugated π system is located closer to the pSB nitrogen, which further promotes the migration of pSB positive charge toward the electron-rich polyene part. A defect around the C14−C15 bond weakens this pathway more significantly in the excited state. As a consequence, the energy gap increases and a blue shift of the absorbed light is observed. The effect will be even stronger when considering that the conjugation defect spreads over a number of adjacent bonds into the isomerization region.

The observed twisting of the polyene chain around C14−C15 is similar to that observed in BR.[54] Since the L105Q mutation reduces the H−C14−C15−H torsion angle only slightly (Figure 7f), its color-tuning contribution is most likely negligible, also taking into account that a higher coplanarity would probably stabilize the excited state over the ground state, resulting in a red shift and not a blue shift.[59]

Effect of the Green−Blue Switch on the Photodynamics of Proteorhodopsin. Aside from explaining the source of the observed blue shift, our NMR data also provide clues for understanding the mutation-induced alterations in PR photodynamics.

The generally slower primary reaction in GPR_{L105Q} (Figure 2a) is most likely a consequence of a conjugation defect in that region, which results in a higher isomerization barrier. This is a direct consequence of the mutation-induced alterations of the retinal structure and electronic configuration caused by surrounding residues such as Q105 and T101. The generation of photocycle intermediates is also strongly affected (Figure 2b). The lifetime of the M state is reduced, indicating faster reprotonation of the Schiff base during the photocycle. In contrast, the decay of the late intermediates N and O is significantly elongated, which accounts for the overall longer photocycle. The decay of these intermediates is associated with the reprotonation of the primary proton donor E108 in helix C, which is close to the mutation site, and involves an outward movement of helix F to support proton uptake from the cytoplasmic side, as known from BR.[69−72] Our data show that significant backbone chemical shift changes induced by this mutation extend toward the cytoplasm to A116 on helix C, which passes E108 (Figure 4). Furthermore, it has been shown for BR that an outward movement of helix F hinged around a Trp residue.[29,73] The corresponding Trp (W197) in PR is affected by residue 105, and this change spreads to other residues (A185, T188, and I194) on the cytoplasmic half of helix F. These local conformational rearrangements appear to be related to the altered lifetime of the N and O intermediate states in the BPR mutant. Indeed, some mutation in these locally affected regions significantly extends the lifetimes of the N and O states in PR.[74] A link between the O-state decay and proton-pumping activity was found by analyzing various PR variants:[74] the slower the O state decays, the less efficient becomes proton pumping. This fact has been linked to the biological activity of BPR.[22] Our data therefore provide a clear structural clue to this functional adaptation.

CONCLUSIONS

Because of their environmental light adaptation, proteorhodopsins are an intriguing class of retinal proteins. Despite their sequence diversity, their blue−green color switch is dominated by the nature-selected single-point mutation L105Q. This makes this group of proteins an ideal showcase for addressing the molecular mechanism of the phenomenon of retinal-based color tuning. By combining high-field MAS NMR for high spectral resolution and DNP for unprecedented sensitivity with properly designed labeling schemes, we were able to probe the structural changes in both the protein and retinal at a site-specific level with high precision. Our data clearly show that the color switch triggers only highly localized structural changes within PR that can be correlated to the slowed photocycle and point to the end of the retinal molecule as the hotspot for the color tuning. Further computational approaches such as QM/MM simulations confined by MAS NMR parameters will enable access to the full electronic configuration of retinal and the surrounding protein environment. Our study also presents an approach for obtaining valuable high-resolution experimental structural information directly correlated to the optical properties of protein−chromophore systems, which could support and complement computational and biochemical/biophysical as well as other structural biology approaches on such important targets.

MATERIALS AND METHODS

Sample Preparation. GPR (eBAC31A08 variant[1]) expression and purification were carried out as described previously.[46] The GPR_{L105Q} gene was kindly provided by Prof. Spudich (The University of Texas Medical School). GPR and GPR_{L105Q} were cloned in a pET27b-plasmid and expressed in *Escherichia coli* C43 cells. U-[^{2}H,^{13}C,^{15}N] GPRs were expressed in the same *E. coli* strain using a protocol modified from Ward et al.[75] A five-step adaptation (LB with 30, 60, and 90% v/v D_2O and M9 with 90 and about 99% D_2O) was performed before expression in perdeuterated medium. A high kanamycin concentration (200 μg/mL) was used in order to stably maintain the plasmid. The starting optical density at 600 nm (OD_{600}) in perdeuterated M9 medium (3−4 g/L U-[^{2}H,^{13}C] glucose and 1−2 g/L $^{15}NH_4Cl$) was 0.14, and cells were incubated for about 10 h at 30 °C (220 rpm) until OD_{600} reached between 0.6 and 0.8. IPTG was then added to reach a concentration of 200 mg/L for induction, together with 35.5 μL of retinal solution (10 mg/mL in EtOH-d_6). The culture was incubated for 12 h under the same conditions, and another batch of retinal solution was added (40 μL). After that, the culture was continued for another 8 h before cell harvesting. The protein was solubilized in 1.5% DDM at 4 °C overnight. The solubilized protein (supernatant) was purified using a Ni-NTA matrix. The bound protein was eluted with 500 mM imidazole in 0.05% DDM. Purity was checked by absorption spectroscopy and SDS-PAGE. In addition, blue native PAGE analysis was carried out (Figure S4 in the Supporting Information). The protein yield for both constructs was about 11 mg/L.

For ssNMR experiments U-[^{13}C,^{15}N] PR was reconstituted in 9:1 DMPC/DMPA liposomes at a protein to lipid ratio of 2:1 (w/w) as previously reported. The proteoliposome was collected by ultracentrifugation and washed intensively in NMR sample buffer containing 50 mM Tris and 5 mM $MgCl_2$ at pH 9. U-[^{2}H,^{13}C,^{15}N] PR was reconstituted into DMPC-d_{67} liposome at a lipid-to-protein ratio of about 20:1. The complete incorporation of PR into deuterated lipids was confirmed by sucrose gradient experiments. The deuterated sample was washed multiple times in fully deuterated NMR sample buffer and then incubated at 4 °C for 2 weeks, during which the buffer was changed at least three times. The pD of the deuterated NMR buffer was calibrated to be equivalent to pH 9.0 as used on the protonated samples in this work.

14,15-^{13}C-all-*trans*-retinal was synthesized as reported previously.[15] It was incorporated into GPR by direct addition to the medium as described before. Reconstituted samples were incubated overnight at 4 °C with 20 mM TOTAPOL in a buffer containing 10% H_2O, 30% glycerol-d_8, and 60% D_2O. The solution was removed carefully, and

dx.doi.org/10.1021/ja5097946 | J. Am. Chem. Soc. 2014, 136, 17578−17590

the pellets were transferred to a 3.2 mm zirconium rotor. Each sample for screening of DNP conditions contained 2.5 mg of protein. For the measurements on 14,15-^{13}C-all-*trans*-retinal-labeled GPR, 2 mg of GPR and 5 mg of GPR_{L105Q} were used.

Optical Spectroscopy. Stationary and time-resolved optical spectroscopy was carried out as described previously.[15] GPR and GPR_{L105Q} were used solubilized in 0.15% DDM, 150 mM NaCl, 50 mM Tris, pH 9. The sample was diluted to an OD of 0.5 (d = 0.1 cm) for pump−probe spectroscopy and to an OD of 0.7 (d = 1 cm) for flash photolysis.

High-Resolution MAS NMR Experiments. All of the high-field MAS NMR spectra for assignment were acquired using standard pulse programs on a Bruker Avance III spectrometer operated at 20 T (850 MHz as the ^{1}H Larmor frequency) equipped with a 4 mm triple-resonance probe. The MAS frequency was stabilized at 10 kHz, and the effective sample temperature was about 4 °C. The mixing time in PDSD experiments was 20 ms. The spectra acquired on GPR and GPR_{L105Q} mutant were processed in the same way.

The ^{1}H−^{13}C MELODI-HETCOR experiment was performed using a pulse sequence similar to the one reported in the literature.[49,76] The MAS frequency was set to 11.26 kHz. ^{1}H−^{13}C dipolar dephasing was achieved in two-rotor periods with a dephasing time of 20 μs. The ^{1}H FSLG homonuclear decoupling[77] field strengths during the dephasing period and the chemical shift encoding period were 92 and 90 kHz, respectively. Data acquisition in the indirect dimension was incremented by 72.6 μs, and a total of 64 t_1 points were collected. A long ^{1}H−^{13}C CP with a contact time of 10 ms was used. SPINAL64[78] decoupling with the B_1 field at about 50 kHz was applied during acquisition. A chemical shift scaling factor of 0.578 was applied in the indirect dimension.

DNP MAS NMR Experiments. All of the DNP MAS NMR experiments were performed on a Bruker Avance II wide-bore spectrometer operated at 392.78 MHz and equipped with a triple-resonance 3.2 mm cryo-MAS probe. A MAS frequency of 8000 ± 2 Hz was used in all of the experiments. The temperature inside the stator was kept at 100 K. Microwaves were generated from a gyrotron (Gycom, Russian Federation) operating at 259 GHz. Energy loss within the probe head was below 2 dB, and the overall decay of microwave energy was about 5 dB from gyrotron to stator. The effective microwave power applied on our NMR samples was about 2 W.

The ^{1}H−^{13}C/^{15}N CP and ^{13}C−^{15}N DCP spectra were acquired using standard pulse sequences with SPINAL64 heteronuclear decoupling at 135 kHz during acquisition.[78] The POST-C7 scheme was used to excite and reconvert DQ coherence.[79] Continuous-wave decoupling at 112 kHz and SPINAL64[78] decoupling at 105 kHz were applied during POST-C7 pulses and acquisition time, respectively. To record DQ buildup curves, the durations of DQ excitation and reconversion periods were varied simultaneously by changing both the numbers of C7 excitation and reconversion cycles in steps of 142.9 μs.[33] Each step was recorded with 512 scans.

The HLF-HCCH experiments were carried out as described by Levitt and co-workers.[53] DQ coherences were excited, evolved under homonuclear proton decoupling, and were detected after a reconversion step. Two complete POST-C7 cycles were used for both DQ excitation and reconversion. The ^{13}C carrier frequency was placed in the middle of the resonating frequencies of C14 and C15. A phase-modulated Lee−Goldburg (PMLG) homonuclear decoupling step[77] with a radiofrequency field of 112 kHz was applied during the DQ evolution time, which was incremented by multiple integers of 18 PMLG cycles (one-eighth of one rotor period). Two equal proton-decoupling periods (112 kHz) were applied before and after the evolution time in order to keep the total evolution time constant (two rotor periods, 250 μs). Typically 1024 to 2048 scans were accumulated for each spectrum.

Spectral Assignments, Spin Dynamics Simulations, and Data Fitting. The analyses of the PDSD, NCA, and N(CA)CX spectra of GPR_{L105Q} were carried out in CARA (cara.NMR.ch) using a reference chemical shift data set of GPR (BMRB 15955, 17817)[14,45] as a starting point. All of the assignments were validated in all spectra and are summarized in Table S1 in the Supporting Information. For further analysis, only unambiguous assignments with chemical shift differences larger than 0.4 ppm were used.

Spin dynamics simulations of DQ buildup and HLF-HCCH dephasing curves were performed using SIMPSON.[80] The ^{1}H−^{1}H and ^{1}H−^{13}C decouplings were treated by turning off the ^{1}H−^{1}H and ^{1}H−^{13}C dipolar interactions. The other details are included in the SIMPSON script in the Supporting Information. A series of DQ buildup curves were calculated by varying the ^{13}C−^{13}C dipolar coupling constant from 2150 Hz (1.52 Å distance) to 3000 Hz (1.36 Å distance). To account for transverse relaxation, DQ buildup curves were multiplied by a monoexponential decay function. Experimental data were analyzed by searching for global minima under variation of bond lengths and the time constant used to describe the exponential decay. Unambiguous minima were obtained for both experimental data sets (Figure 7c). In order to simulate the HLF-HCCH data, a library of HCCH conformers was created by varying the dihedral angle in steps of 1° using PYMOL (Schrödinger LLC). The complete parameters used to describe the spin system are given in the Supporting Information. The appropriate C14−C15 bond lengths determined from the DQ buildup curves were used. For each of the resulting HCCH conformers, a dephasing curve was calculated. The experimentally observed transverse relaxation was taken into account through multiplication by a monoexponentially decaying function. The best-fit solution was searched through a backward iterative optimization of both the dephasing curve and the exponential decay. Python and shell programming scripts were used to automate simulation and numerical optimization. As a control, additional simulations were carried out, which included an additional ^{15}N and ^{1}H at the Schiff base position. Their effects on the dephasing curves were negligible.

■ ASSOCIATED CONTENT

Supporting Information

Comparison of PDSD and NCA spectra of GPR and GPR_{L105Q} (Figure S1); supporting data for ^{1}H−^{13}C HETCOR experiments on [U-^{13}C,^{2}H] GPR and GPR_{L105Q} (Figure S2); DNP spin−echo experiments on [14,15-^{13}C-all-*trans*-retinal] GPR (Figure S3); Blue native gels of GPR and GPR_{L105Q} in DDM micelles and liposomes (Figure S4); table of resonance assignments and list of chemical shift changes (Table S1); and SIMPSON script for HLF-HCCH spin simulations. This material is available free of charge via the Internet at http://pubs.acs.org.

■ AUTHOR INFORMATION

Corresponding Author

glaubitz@em.uni-frankfurt.de

Notes

The authors declare no competing financial interest.

■ ACKNOWLEDGMENTS

The work was funded by DFG/SFB 807 “Transport and Communication across Membranes”. The DNP experiments were enabled through an equipment grant provided by the DFG (GL 307/4-1 and Cluster of Excellence Macromolecular Complexes Frankfurt). We are grateful to Igor Schapiro (MPI Chemical Energy Conversion) for helpful discussions and initial QM/MM calculations. Vasyl Denysenkov and Jörn Plackmeier (University of Frankfurt) are acknowledged for their help in establishing the DNP setup and in TOTAPOL synthesis. Marie Concistre and Malcolm H. Levitt are acknowledged for initial advice on the HCCH data analysis. Leonardo Gonnelli and Gianluca Gallo (CERM, Florence) are acknowledged for valuable and practical suggestions on protein perdeuteration.

REFERENCES

(1) Beja, O.; Aravind, L.; Koonin, E. V.; Suzuki, M. T.; Hadd, A.; Nguyen, L. P.; Jovanovich, S. B.; Gates, C. M.; Feldman, R. A.; Spudich, J. L.; Spudich, E. N.; DeLong, E. F. *Science* **2000**, *289*, 1902.
(2) Hoffmann, J.; Aslimovska, L.; Bamann, C.; Glaubitz, C.; Bamberg, E.; Brutschy, B. *Phys. Chem. Chem. Phys.* **2010**, *12*, 3480.
(3) Klyszejko, A. L.; Shastri, S.; Mari, S. A.; Grubmuller, H.; Muller, D. J.; Glaubitz, C. *J. Mol. Biol.* **2008**, *376*, 35.
(4) Beja, O.; Spudich, E. N.; Spudich, J. L.; Leclerc, M.; DeLong, E. F. *Nature* **2001**, *411*, 786.
(5) de la Torre, J. R.; Christianson, L. M.; Beja, O.; Suzuki, M. T.; Karl, D. M.; Heidelberg, J.; DeLong, E. F. *Proc. Natl. Acad. Sci. U.S.A.* **2003**, *100*, 12830.
(6) DeLong, E. F. *Nature* **2009**, *459*, 200.
(7) Friedrich, T.; Geibel, S.; Kalmbach, R.; Chizhov, I.; Ataka, K.; Heberle, J.; Engelhard, M.; Bamberg, E. *J. Mol. Biol.* **2002**, *321*, 821.
(8) Gómez-Consarnau, L.; Akram, N.; Lindell, K.; Pedersen, A.; Neutze, R.; Milton, D. L.; Gonzälez, J. M.; Pinhassi, J. *PLoS Biol.* **2010**, *8*, No. e1000358.
(9) Gómez-Consarnau, L.; González, J. M.; Coll-Lladó, M.; Gourdon, P.; Pascher, T.; Neutze, R.; Pedrós-Alió, C.; Pinhassi, J. *Nature* **2007**, *445*, 210.
(10) Huber, R.; Köhler, T.; Lenz, M. O.; Bamberg, E.; Kalmbach, R.; Engelhard, M.; Wachtveitl, J. *Biochemistry* **2005**, *44*, 1800.
(11) Bergo, V.; Amsden, J. J.; Spudich, E. N.; Spudich, J. L.; Rothschild, K. J. *Biochemistry* **2004**, *43*, 9075.
(12) Reckel, S.; Gottstein, D.; Stehle, J.; Löhr, F.; Verhoefen, M.-K.; Takeda, M.; Silvers, R.; Kainosho, M.; Glaubitz, C.; Wachtveitl, J.; Bernhard, F.; Schwalbe, H.; Güntert, P.; Dötsch, V. *Angew. Chem., Int. Ed. Engl.* **2011**, *50*, 11942.
(13) Hempelmann, F.; Hölper, S.; Verhoefen, M.-K.; Woerner, A. C.; Köhler, T.; Fiedler, S.-A.; Pfleger, N.; Wachtveitl, J.; Glaubitz, C. *J. Am. Chem. Soc.* **2011**, *133*, 4645.
(14) Shi, L.; Lake, E. M.; Ahmed, M. A.; Brown, L. S.; Ladizhansky, V. *Biochim. Biophys. Acta* **2009**, *1788*, 2563.
(15) Mehler, M.; Scholz, F.; Ullrich, S. J.; Mao, J.; Braun, M.; Brown, L. J.; Brown, R. C.; Fiedler, S. A.; Becker-Baldus, J.; Wachtveitl, J.; Glaubitz, C. *Biophys. J.* **2013**, *105*, 385.
(16) Stone, K. M.; Voska, J.; Kinnebrew, M.; Pavlova, A.; Junk, M. J. N.; Han, S. G. *Biophys. J.* **2013**, *104*, 472.
(17) Ran, T.; Ozorowski, G.; Gao, Y.; Sineshchekov, O. A.; Wang, W.; Spudich, J. L.; Luecke, H. *Acta Crystallogr., Sect. D* **2013**, *69*, 1965.
(18) Bamann, C.; Bamberg, E.; Wachtveitl, J.; Glaubitz, C. *Biochim. Biophys. Acta* **2014**, *1837*, 614.
(19) Man, D.; Wang, W.; Sabehi, G.; Aravind, L.; Post, A. F.; Massana, R.; Spudich, E. N.; Spudich, J. L.; Beja, O. *EMBO J.* **2003**, *22*, 1725.
(20) Bamann, C.; Nagel, G.; Bamberg, E. *Curr. Opin. Neurobiol.* **2010**, *20*, 610.
(21) Kelemen, B. R.; Du, M.; Jensen, R. B. *Biochim. Biophys. Acta* **2003**, *1618*, 25.
(22) Wang, W. W.; Sineshchekov, O. A.; Spudich, E. N.; Spudich, J. L. *J. Biol. Chem.* **2003**, *278*, 33985.
(23) Amsden, J. J.; Kralj, J. M.; Bergo, V. B.; Spudich, E. N.; Spudich, J. L.; Rothschild, K. J. *Biochemistry* **2008**, *47*, 11490.
(24) Hillebrecht, J. R.; Galan, J.; Rangarajan, R.; Ramos, L.; McCleary, K.; Ward, D. E.; Stuart, J. A.; Birge, R. R. *Biochemistry* **2006**, *45*, 1579.
(25) Kralj, J. M.; Bergo, V. B.; Amsden, J. J.; Spudich, E. N.; Spudich, J. L.; Rothschild, K. J. *Biochemistry* **2008**, *47*, 3447.
(26) Kralj, J. M.; Spudich, E. N.; Spudich, J. L.; Rothschild, K. J. *J. Phys. Chem. B* **2008**, *112*, 11770.
(27) Maiti, T. K.; Yamada, K.; Inoue, K.; Kandori, H. *Biochemistry* **2012**, *51*, 3198.
(28) Ozaki, Y.; Kawashima, T.; Abe-Yoshizumi, R.; Kandori, H. *Biochemistry* **2014**, *53*, 6032.
(29) Subramaniam, S.; Greenhalgh, D. A.; Rath, P.; Rothschild, K. J.; Khorana, H. G. *Proc. Natl. Acad. Sci. U.S.A.* **1991**, *88*, 6873.
(30) Haeckel, M.; Hinz, H.-J.; Hedwig, G. R. *Biophys. Chem.* **1999**, *82*, 35.
(31) Zamyatnin, A. A. *Annu. Rev. Biophys* **1984**, *13*, 145.
(32) Wang, S.; Ladizhansky, V. *Prog. Nucl. Magn. Reson. Spectrosc.* **2014**, *82*, 1.
(33) Carravetta, M.; Eden, M.; Johannessen, O. G.; Luthman, H.; Verdegem, P. J. E.; Lugtenburg, J.; Sebald, A.; Levitt, M. H. *J. Am. Chem. Soc.* **2001**, *123*, 10628.
(34) Spooner, P. J. R.; Sharples, J. M.; Goodall, S. C.; Seedorf, H.; Verhoeven, M. A.; Lugtenburg, J.; Bovee-Geurts, P. H. M.; DeGrip, W. J.; Watts, A. *Biochemistry* **2003**, *42*, 13371.
(35) Carravetta, M.; Zhao, X.; Johannessen, O. G.; Lai, W. C.; Verhoeven, M. A.; Bovee-Geurts, P. H. M.; Verdegem, P. J. E.; Kiihne, S.; Luthman, H.; de Groot, H. J. M.; deGrip, W. J.; Lugtenburg, J.; Levitt, M. H. *J. Am. Chem. Soc.* **2004**, *126*, 3948.
(36) Jaroniec, C. P.; Lansing, J. C.; Tounge, B. A.; Belenky, M.; Herzfeld, J.; Griffin, R. G. *J. Am. Chem. Soc.* **2001**, *123*, 12929.
(37) Etzkorn, M.; Martell, S.; Andronesi, O. C.; Seidel, K.; Engelhard, M.; Baldus, M. *Angew. Chem., Int. Ed.* **2007**, *46*, 459.
(38) Higman, V. A.; Varga, K.; Aslimovska, L.; Judge, P. J.; Sperling, L. J.; Rienstra, C. M.; Watts, A. *Angew. Chem., Int. Ed.* **2011**, *50*, 8432.
(39) Wang, S.; Munro, R. A.; Shi, L.; Kawamura, I.; Okitsu, T.; Wada, A.; Kim, S. Y.; Jung, K. H.; Brown, L. S.; Ladizhansky, V. *Nat. Methods* **2013**, *10*, 1007.
(40) Ni, Q. Z.; Daviso, E.; Can, T. V.; Markhasin, E.; Jawla, S. K.; Swager, T. M.; Temkin, R. J.; Herzfeld, J.; Griffin, R. G. *Acc. Chem. Res.* **2013**, *46*, 1933.
(41) Bajaj, V. S.; Mak-Jurkauskas, M. L.; Belenky, M.; Herzfeld, J.; Griffin, R. G. *Proc. Natl. Acad. Sci. U.S.A.* **2009**, *106*, 9244.
(42) Jacso, T.; Franks, W. T.; Rose, H.; Fink, U.; Broecker, J.; Keller, S.; Oschkinat, H.; Reif, B. *Angew. Chem., Int. Ed.* **2012**, *51*, 432.
(43) Ong, Y. S.; Lakatos, A.; Becker-Baldus, J.; Pos, K. M.; Glaubitz, C. *J. Am. Chem. Soc.* **2013**, *135*, 15754.
(44) Pfleger, N.; Lorch, M.; Woerner, A. C.; Shastri, S.; Glaubitz, C. *J. Biomol. NMR* **2008**, *40*, 15.
(45) Shi, L.; Ahmed, M. A.; Zhang, W.; Whited, G.; Brown, L. S.; Ladizhansky, V. *J. Mol. Biol.* **2009**, *386*, 1078.
(46) Yang, J.; Aslimovska, L.; Glaubitz, C. *J. Am. Chem. Soc.* **2011**, *133*, 4874.
(47) Sharaabi, Y.; Brumfeld, V.; Sheves, M. *Biochemistry* **2010**, *49*, 4457.
(48) Kiihne, S. R.; Creemers, A. F. L.; de Grip, W. J.; Bovee-Geurts, P. H. M.; Lugtenburg, J.; de Groot, H. J. M. *J. Am. Chem. Soc.* **2005**, *127*, 5734.
(49) Yao, X. L.; Schmidt-Rohr, K.; Hong, M. *J. Magn. Reson.* **2001**, *149*, 139.
(50) Song, C. S.; Hu, K. N.; Joo, C. G.; Swager, T. M.; Griffin, R. G. *J. Am. Chem. Soc.* **2006**, *128*, 11385.
(51) Verhoefen, M.-K.; Schäfer, G.; Shastri, S.; Weber, I.; Glaubitz, C.; Mäntele, W.; Wachtveitl, J. *Biochim. Biophys. Acta* **2011**, *1807*, 1583.
(52) Hamanaka, T.; Kakudo, M.; Ashida, T.; Mitsui, T. *Acta Crystallogr., Sect. B* **1972**, *28*, 214.
(53) Concistre, M.; Johannessen, O. G.; McLean, N.; Bovee-Geurts, P. H.; Brown, R. C.; DeGrip, W. J.; Levitt, M. H. *J. Biomol. NMR* **2012**, *53*, 247.
(54) Lansing, J. C.; Hohwy, M.; Jaroniec, C. P.; Creemers, A. F. L.; Lugtenburg, J.; Herzfeld, J.; Griffin, R. G. *Biochemistry* **2002**, *41*, 431.
(55) Yoshizawa, S.; Kumagai, Y.; Kim, H.; Ogura, Y.; Hayashi, T.; Iwasaki, W.; DeLong, E. F.; Kogure, K. *Proc. Natl. Acad. Sci. U.S.A.* **2014**, *111*, 6732.
(56) Kloppmann, E.; Becker, T.; Ullmann, G. M. *Proteins: Struct., Funct., Bioinf.* **2005**, *61*, 953.
(57) Mathies, R.; Stryer, L. *Proc. Natl. Acad. Sci. U.S.A.* **1976**, *73*, 2169.
(58) Schenkl, S.; van Mourik, F.; van der Zwan, G.; Haacke, S.; Chergui, M. *Science* **2005**, *309*, 917.
(59) Yan, B.; Spudich, J. L.; Mazur, P.; Vunnam, S.; Derguini, F.; Nakanishi, K. *J. Biol. Chem.* **1995**, *270*, 29668.

(60) Hu, J. G. G.; Sun, B. Q. Q.; Petkova, A. T.; Griffin, R. G.; Herzfeld, J. *Biochemistry* **1997**, *36*, 9316.
(61) Hu, J. G. G.; Griffin, R. G.; Herzfeld, J. *J. Am. Chem. Soc.* **1997**, *119*, 9495.
(62) Buda, F.; deGroot, H. J. M.; Bifone, A. *Phys. Rev. Lett.* **1996**, *77*, 4474.
(63) Verhoeven, M. A.; Creemers, A. F. L.; Bovee-Geurts, P. H. M.; De Grip, W. J.; Lugtenburg, J.; de Groot, H. J. M. *Biochemistry* **2001**, *40*, 3282.
(64) Creemers, A. F. L.; Bovee-Geurts, P. H. M.; DeGrip, W. J.; Lugtenburg, J.; de Groot, H. J. M. *Biochemistry* **2004**, *43*, 16011.
(65) Melaccio, F.; Ferre, N.; Olivucci, M. *Phys. Chem. Chem. Phys.* **2012**, *14*, 12485.
(66) Fujimoto, K.; Hayashi, S.; Hasegawa, J.; Nakatsuji, H. *J. Chem. Theory Comput.* **2007**, *3*, 605.
(67) Fujimoto, K. J.; Asai, K.; Hasegawa, J. *Phys. Chem. Chem. Phys.* **2010**, *12*, 13107.
(68) Lee, H. M.; Kim, J.; Kim, C. J.; Kim, K. S. *J. Chem. Phys.* **2002**, *116*, 6549.
(69) Subramaniam, S.; Henderson, R. *Nature* **2000**, *406*, 653.
(70) Lanyi, J. K.; Luecke, H. *Curr. Opin. Struct. Biol.* **2001**, *11*, 415.
(71) Hirai, T.; Subramaniam, S. *PLoS One* **2009**, *4*, No. e5769.
(72) Vonck, J. *EMBO J.* **2000**, *19*, 2152.
(73) Kuhlbrandt, W. *Nature* **2000**, *406*, 569.
(74) Kim, S. Y.; Waschuk, S. A.; Brown, L. S.; Jung, K. H. *Biochim. Biophys. Acta* **2008**, *1777*, 504.
(75) Ward, M. E.; Shi, L.; Lake, E.; Krishnamurthy, S.; Hutchins, H.; Brown, L. S.; Ladizhansky, V. *J. Am. Chem. Soc.* **2011**, *133*, 17434.
(76) Yao, X. L.; Hong, M. *J. Biomol. NMR* **2001**, *20*, 263.
(77) Vinogradov, E.; Madhu, P. K.; Vega, S. *Chem. Phys. Lett.* **1999**, *314*, 443.
(78) Fung, B. M.; Khitrin, A. K.; Ermolaev, K. *J. Magn. Reson.* **2000**, *142*, 97.
(79) Hohwy, M.; Jakobsen, H. J.; Eden, M.; Levitt, M. H.; Nielsen, N. C. *J. Chem. Phys.* **1998**, *108*, 2686.
(80) Bak, M.; Rasmussen, J. T.; Nielsen, N. C. *J. Magn. Reson.* **2000**, *147*, 296.
(81) Hu, J.; Griffin, R. G.; Herzfeld, J. *Proc. Natl. Acad. Sci. U.S.A.* **1994**, *91*, 8880.